Online Modeling of *In Vivo* Mechanical Properties of Soft Tissue for Robotic Surgery

BIOEN 402 Final Report

Written by Andrew John Hill
Submitted June 6, 2012

Primary Investigators:
Professor Howard Chizeck , Dept. of Electrical Engineering
Professor Blake Hannaford, Dept. of Electrical Engineering

Abstract:
Minimally invasive surgical (MIS) techniques, such as laparoscopic surgery (performed through small incisions using specialized tools), are an integral part of modern medicine and the future of surgery. Technologically advanced tools such as MIS robots are promising to replace or augment existing MIS manual tools. MIS robots improve on manual surgery, as they can incorporate increasingly sophisticated features such as force feedback for surgeons, automatic identification of diseased tissues, and partial automation of surgical tasks. These features can reduce patient pain, recovery time and thus healthcare costs by eliminating unintended damage to tissue and providing surgeons with tools to perform surgery more effectively. Each of these new features either requires or would greatly benefit from an accurate mathematical description of the dynamic mechanical properties for the tissues with which surgeons interact. Dynamic tissue property quantification requires that we apply a range of forces to the tissue and measure the resulting displacements. A device capable of collecting the necessary data to obtain an equation relating applied force to tissue displacement for any tissue of interest designed, built, and calibrated. An advanced signal processing and system identification algorithm (unscented Kalman filtering), has been used to evaluate fits to collected data recursively over time. This will allow accurate results to be maintained as the tissue properties change over time. This device has been used to collect data from phantom tissue ad *in vivo* abdominal organs in pigs. In addition to being an important study that has not been performed in the literature, the ability to carry out real-time collection and analysis of the *in vivo* data could provide a significant step toward partially automating surgery.

Acknowledgements

First and foremost I would like to thank my two advisors, Professor Howard Chizeck and Professor Blake Hannaford for their patience, guidance, and encouragement throughout the course of this capstone project. In addition to their direct support of my project, they have provided me with invaluable mentorship, career advice, and extensive exposure to many components of academic research. I have also been able to attend several qualifying exams, general exams, final exams, and events such as the Robotics Research Colloquium, which have been tremendously inspiring and educational as a developing scientist and engineer.

I would also like to thank Ph.D. Candidate Sina Nia Kosari for his guidance and mentorship throughout this project. I also had the opportunity to take his course on Haptic Enabled Devices, a graduate level course in the Electrical Engineering Department. He performed extremely well in teaching his first course and I wish him the best of luck in pursuing a professorship in the future.

Thank you to Levi Cheng, Hawkeye King, Lee White, and Fredrick Ryden, for their technical support throughout the course of my project.

Thank you to everyone in the Biorobotics Lab and all my friends in the Department of Bioengineering for making my time here so enjoyable! I would especially like to thank Tim Kowalewski, who was the first person I worked with in the BRL. Tim is a fantastic teacher and mentor and I wish him luck as a professor at the University of Minnesota!

I would like to acknowledge the bioengineering staff, especially Dr. Chris Neils, Dr. Alyssa Taylor, Department Chair Paul Yager, and Kelli Jayn Nichols for their invaluable support and mentorship throughout my time in the department.

I would like to acknowledge the Mary Gates Endowment for my Mary Gates Research Award and the URP staff for their aid in coordinating my presentation at the UW Undergraduate Research Symposium.

Thank you to my family Roger Hill, Leslie Hill, and Ian Hill for their love and support throughout my time at the University of Washington (and before). I truly could not have done it without them and I am glad that I will be able to visit more often through my next couple years in Boston!

Thank you to my lovely girlfriend, Molly Gasperini for her love and support over the past two years. I am so happy that I will have her with me as I begin this next challenging chapter in my life and career as an engineer.

Table of Contents

Introduction

Definition of the Project

The goal of my project was to develop a device that performs online model identification of soft tissue by applying a range of known forces to the tissue with a circular indenter, measuring the resulting tissue displacements, and analyzing the data in real time. In addition to the phantom (artificial) tissue used in initial testing, *in vivo* porcine liver tests were used, as it has been shown to have similar mechanical properties to that of human liver [1]. Liver tissue was used because it is an organ commonly operated on in procedures in minimally invasive surgery (MIS) [1]. Phase one involved developing the device and calibrating it correctly. Phase two involved performing online model identification on phantom tissue. Phase three involved performing online model identification of *in vivo* porcine liver.

In order to achieve online (a less restrictive version of real-time) model identification the device must be able to reliably apply a known force to the soft tissue, accurately measure the resulting displacement of the soft tissue, and collect the force-displacement data points for analysis on a host PC. The host PC must be capable of collecting the incoming data and performing recursive analysis. Collectively, this system must perform these tasks with minimal latency to be useful in real-time systems. One of the goals of this project was to validate the performance of the individual system components and to ensure that the data analysis consistently produces a good fit to the dataset.

There are a number of different mathematical models for soft tissue dynamics that have been examined in literature, such as 2nd order and higher polynomials, the Kelvin-Voigt model ($\hat{f} = \hat{x}_0 + \hat{k}x + \hat{b}\dot{x}$), and the Hunt-Crossley model ($\hat{f} = \hat{x}_0 + \hat{k}x^{\hat{n}} + \hat{\lambda}x^{\hat{n}}\dot{x}$) [1]. My project also sought to evaluate three of these models with respect to their accuracy and computational complexity. An additional goal of the project was to identify the model that provides the best ratio of accuracy to computational complexity to validate its utility in online model identification.

The products of this project have the potential to benefit a number of applications in the field of robotic surgery such as force feedback for surgeons, control algorithms for surgical robots, increased precision of robotic surgery, and partial automation of surgical tasks.

Medical and Scientific Significance

Research in robotic surgery is leading to the incorporation of increasingly sophisticated features such as force feedback, control algorithms, increased precision, and partial automation of tasks, which will continue to improve modern surgery. Each of these features would require or greatly benefit from accurate quantification of the dynamic mechanical properties of soft tissue.

For example, because surgical robots do not currently provide force-feedback to the surgeon and different surgical tools scale forces differently, excessive forces are often applied during surgery, leading to unnecessary tissue damage. This is an issue particularly with inexperienced or resident surgeons. Two potential solutions to this current problem in robotic surgery are to implement force feedback and to implement partial automation of grasping with a controller. In the force feedback solution, the tissue model provided by my device would predict the forces involved throughout the act of grasping, allowing accurate force-feedback to the surgeon. In the controller solution, the tissue model provided by my device would be part of the control loop. Figure 1 shows how this model could be used in a Model Predictive Control loop.

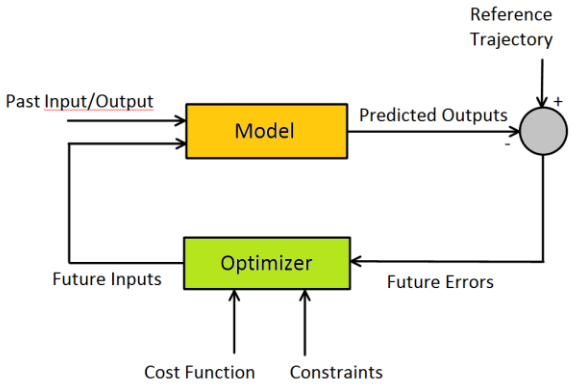

Figure 1: Flow diagram of a model predictive control system [2]

Model predictive control would allow for incorporation of dynamic tissue models into control loops, potentially increasing accuracy of control when surgical robots are in contact with soft tissues during surgery. Many of these new features have the potential to reduce the learning curve of robotic surgery to reduced medical costs to both the patient and hospitals due to decreased recovery time and incidence of complications.

This device could be used to perform further studies to test other tissues, expanding the library of available data. Eventually, with the appropriate approval, similar studies could be conducted to examine the properties of human tissues. The developed models could then be used in human surgical procedures.

The device design includes a replaceable circular end to the indenter, allowing for additional studies to be performed on tissues with different indenter shapes and sizes. Another potential application of this device is the study of the forces involved in needle retraction, another area where use of partial automation could be used in robotic surgery.

Social, Ethical, and Economic Issues

Social and Ethical Issues

The most significant social issue surrounding surgical robots is their safety. Patients could potentially be concerned that malfunction of the robots could have negative results during surgery. Talamani *et al*. conducted a study on the safety and efficacy of robotic surgery in conjunction with the Academic Robotics Group [3]. The study concluded that, "The results of robotic-assisted surgery compare favorably with respect to mortality, complications, and length of stay. Robotic-assisted surgery is safe and effective and is a new reality for American surgery. The role of these devices in surgery will expand as the technology evolves" [3]. In addition, machine failure never resulted in additional damage to the patient. Therefore, while the safety of robotic surgery is constantly being improved, there is no substantiated reason for patient concern regarding the robustness of its design. A marketing campaign may need to take place to promote robotic surgery in the United States.

FDA approval would be required for new features such as the addition of grasping control by demonstrating the safety and robustness of the control. The ethics regarding animal testing is also a concern for this project, due to the use of live pigs. Proper IACUC protocol were followed to uphold the ethical standards of this study. The ethical issue of human testing also acts as a barrier to the creation of human tissue models.

Economic Issues

Unnecessary damage to tissues caused by excessive force can lead to complications for patients [4]. This results in increased medical expenses and increased length of hospital stays, which can cost several thousands of dollars per person per day. Additional treatment to correct complications adds additional expenses for both the patient and hospital. Unfortunately, the cost of a da Vinci Surgical System, as of 2009, was about $1.2 million, with 138,000 in annual maintenance costs [5]. Additional training and equipment add to the startup cost for robotic surgery facilities. This high cost acts as an obstacle to widespread implementation of robotic surgery. While it is known that certain, more complex, procedures cannot be performed without the aid of robotic surgery, the cost benefit for routine minimally invasive surgery has not been proven [3]. It is likely that more widespread use of surgical robots and advancement of the technology will decrease the overall cost of robotic surgery.

Incorporation of the online model identification in robotic controls would help to eliminate damage caused by the application of excessive grasping force during surgery. Such a system would be relatively inexpensive to implement in surgical robots control systems. By limiting damage and complications caused during surgery, the length of hospital stays and number of additional procedures could be reduced.

Technical Background

Tissue Mechanics

Tissue properties, in addition to being highly nonlinear, have been observed to be viscoelastic, meaning that they have both viscous and elastic properties when they are deformed. These viscoelastic properties make tissue properties much more difficult to

accurately model. A material is considered to be viscoelastic if it exhibits any of the three phenomena- hysteresis, creep, and relaxation [6].

Elastic materials by definition, store all of the energy imparted in deformation. However, due to the additional viscous properties in viscoelastic tissues, some energy is dissipated. This leads to a phenomenon known as hysteresis, which causes the unloading portion of the stress strain-curve to be lower than the loading portion of the curve due to the loss in energy [6]. This relationship is shown in Figure 2.

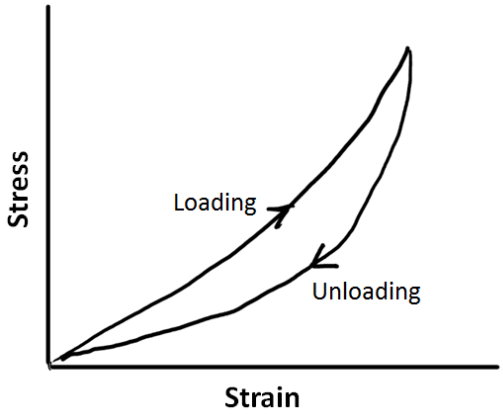

Figure 2: Hysteresis loop observed during loading and unloading of viscoelastic materials.

Elastic materials will maintain a constant strain in response to a constant stress. However, due to the phenomenon known as creep, the strain of viscoelastic materials under a constant stress will continue to increase over time. Eventually, a steady state value of strain will be reached. Similarly, elastic materials will maintain a constant stress at a constant level of strain. Due to a third phenomenon referred to as relaxation, viscoelastic materials will experience a decrease in stress over time at a constant strain [6].

The net product of these effects is that the stress-stain characteristics are time dependent, adding significantly increased complexity when modeling viscoelastic materials. There are a number of different mathematical models of soft tissue that have been examined in literature. These include 2nd order and higher polynomials, the Kelvin-Voigt model ($\hat{f} = \hat{x}_0 + \hat{k}x + \hat{b}\dot{x}$), and the Hunt-Crossley model ($\hat{f} = \hat{x}_0 + \hat{k}x^{\hat{n}} + \hat{\lambda}x^{\hat{n}}\dot{x}$) [7]. While the Kelvin Voigt model, a spring and damper in parallel, somewhat accurately characterizes tissues, the nonlinear Hunt-Crossley model accounts for the energy loss during indenter-

tissue contact. However, this increased accuracy comes at the expense of increased computational complexity.

Model Parameter Identification

The parameters of these models can be fit using the force-displacement data generated by my device. In batch processing this can be performed with the curve fitting utilities in MATLAB. However, for online model identification, recursive methods must be used. One common method of doing this is the recursive least squares method [8]. In this project, I have used a different technique for state estimation called a Kalman Filter. Kalman filters allow for computationally efficient identification of nonlinear-model parameters (that is, tissue properties) and, simultaneously, states of a dynamic system (like robot position). This dual functionality makes Kalman filters will be more useful for incorporating online model identification into a more complex system such as a controller. The two options for nonlinear Kalman filtering are the Extended Kalman Filter (EKF) and the Unscented Kalman Filter (UKF) [9]. The EKF approximates the state distribution using a Gaussian random variable. The portion of the system around the current state is then approximated as a linear function through calculation of the Jacobian matrix. Using analytical techniques, the Gaussian random variable is then propagated through the linear approximation. In highly nonlinear systems, this can cause large errors and corresponding degradation of performance [9].

The UKF remedies this by instead choosing a set of sample points to represent the system to capture the true nonlinear nature of the system. The Gaussian random variable is instead propagated through this non-linear system instead of the linearized approximation, leading to more accurate results for highly nonlinear systems [9]. Also, because the UKF does not require linear approximation of the system, no Jacobian or Hessian matrices need be explicitly calculated, which would be computationally expensive for complex functions. Despite the increase in performance, the EKF and UKF have the same order of computational complexity [9]. A UFK software package is used in this project due to the high degree of nonlinearity observed in soft tissues.

Literature Review

There are a number of different mathematical soft tissue models that have been examined in literature, such as 2nd order and higher polynomials, the Kelvin-Voigt model ($\hat{f} = \hat{x}_0 + \hat{k}x + \hat{b}\dot{x}$), and the Hunt-Crossley model ($\hat{f} = \hat{x}_0 + \hat{k}x^{\hat{n}} + \hat{\lambda}x^{\hat{n}}\dot{x}$) [7]. Several studies have shown that the Hunt-Crossley model is typically the most accurate in replicating the viscoelastic properties of soft tissue because it accounts for the energy lost during contact with the tissue [7, 10]. However, it does this at the expense of computational complexity.

The two main categories of devices that appear in literature for measuring the properties of soft tissue are dynamic mechanical analysis and transient elastography [11, 12]. Somewhat less common approaches that have been found are a torsional resonator device [13] and a mechano-acoustic indenter system [14]. Previous studies in literature suggest that use of different indenter shapes, including studies on needle insertion and retraction, are relevant and could prove useful for applications in robotic surgery [4, 15-17].

Both dynamic mechanical analysis and transient elastography have been shown to have comparable results [11]. The computational complexity of dynamic mechanical analysis is generally less than that of elastography [7, 12], potentially making it more suitable for real-time applications. There have been a number of different dynamic mechanical analysis devices in literature.

A study conducted by Carter *et al.* examined the estimation of tissue parameters of *in vivo* tissues using a hand held indenter device [18]. This hand held device is capable of making force vs. displacement measurements in both *ex vivo* and *in vivo* tissue (Figure 3).

Figure 3: Handheld indenter device [18]

Carter *et al.* provides a good example of a portable device that would be capable of making *in vivo* measurements. The 4.5mm tip and 5N- load cell load cell are moved using a drive wheel and drive thread and the displacement is measured using a linear variable differential transformer (labeled LDVT in Figure 3). Force is then measured using a 5N load-cell. Displacement is measured relative to the reference ring and the trigger button is used to start and stop data collection. However, this study did not perform online model identification, instead focusing on the static properties of soft tissues. *In vivo* studies were performed at very low levels of force, so this study also failed to examine model validation at higher levels of force.

Another dynamic tissue measurement system was implemented by Yamamoto [1]. Yamamoto investigated the application of tissue models in teleoperated surgical systems [1]. In this study, real time model identification using the non-linear Hunt-Crossley tissue model was carried out during palpitation of *in vitro* porcine liver and kidney, using the apparatus shown in Figure 4.

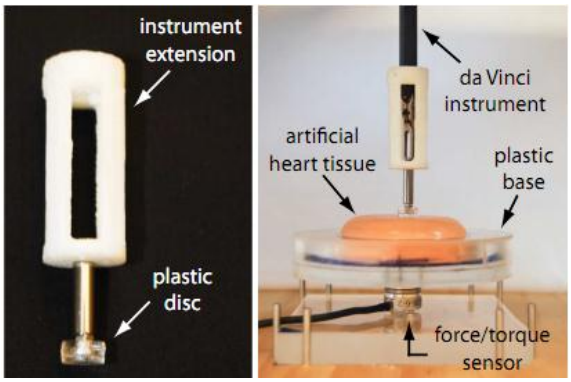

Figure 4: Measurement technique used by Yamamoto [1]

Yamamoto *et al.* used a da Vinci® surgical instrument to apply force with a plastic disc (attached via the instrument extension pictured on the left) and to measure displacement. The force/torque sensor measures how much force has been applied to the tissue. In this case, Yamamoto performed initial experiments on artificial heart tissue. It would be difficult to use this device to make measurements of *in vivo* tissue because the tissue must be placed on the force plate in order to acquire data. Similar existing designs such as by An *et al*. [19], Schwartz *et al*. [17], and Tay *et al.* [20] also appear to be unsuitable for *in vivo* measurements, but have certain components that may help in developing my own design. However, Yamamoto's study did make use of both the least squares and recursive least squares method to implement batch and online model identification.

De *et al.* did research to evaluate the grasping force and grasping durations that could be safely used on porcine liver, ureter, and small bowel without causing damage [4]. In order to apply known forces to the tissue, a motorized endoscopic grasper was developed (Figure 5).

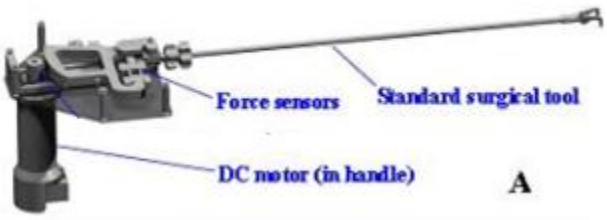

Figure 5: CAD rendering of a motorized endoscopic grasper [4]

A standard surgical grasping tool was fitted with a DC motor and force sensors. The position of the grasper jaws can be calculated using an encoder attached to the DC motor. The force applied by the grasper was calibrated using springs of known stiffness and the damage was quantified using a number of histological assays to measure cell death, inflammation, and activation of the coagulation cascade. An example of visual damage resulting from excessive force is shown in Figure 6.

Figure 6: Photograph of resulting porcine hepatic tissue response to increasing load [4]

The arrows indicate the points at which force was applied (increases in the counter clockwise direction). Note that the points of high stress show a significantly more damage (indicated by dark coloration). The results indicated that there is a nonlinear response between the applied grasping force and tissue damage. This study is significant because the motorized endoscopic grasper device used in this study is very similar to the device required for my project. However, concerns have been raised regarding the appropriateness of this particular device for developing an accurate mathematical model of the tissue [21]. In particular, the surface area of the grasping device is poorly defined and the cable-driven systems may produce a significant error. Cable-driven systems have substantial friction and the cables tend to stretch slightly under load. While error produced by these factors would not have significantly impacted the results of De's study, they would result in inaccurate determination of mechanical tissue properties.

Other studies, including those by Roan *et al*. [22] and Rosen *et al*. [23] used a very similar design for a motorized endoscopic grasper. Rosen *et al*. examined the mechanical properties of a number of porcine tissues *post mortem* and *in vivo*. However, only static (stress-strain) properties were examined. While much of the testing protocol is similar, the

device in this work must be capable of measuring the dynamic (force-displacement) properties of the tissue, in order to create an appropriate mathematical model for control applications.

There are several different options for model parameter identification. Some approaches in literature have utilizes a technique called finite element analysis to obtain tissue parameters [14, 18, 24, 25]. While finite element analysis has been shown to provide accurate results, it is computationally expensive and is not suitable for online applications. Recursive least squares techniques have also been examined in literature [7, 26]. Perhaps the most attractive model identification technique is Kalman filtering; particularly extended Kalman filters and unscented Kalman filters, which are suitable for non-linear systems. The main advantage of a Kalman Filter is that it allows for computationally efficient identification of model parameters (that is, tissue properties) and, simultaneously, states of a dynamic system (like robot position). This allows the online modeling to be easily incorporated into more complex systems such as a controller. Of the two nonlinear varieties, studies in literature suggest that unscented Kalman filters are the most suitable for estimation of highly nonlinear system parameters [9, 27-30]. One reason for this is that the unscented Kalman filters are less prone to error when the system is highly nonlinear, while maintaining the same order of computational complexity of an extended Kalman filter.

Previous Relevant Work in the Biorobotics Laboratory

During Winter Quarter 2011 another undergraduate researcher, Jack Chan, and I worked on modifying several open source non-linear optimization packages for use in model predictive control (MPC) systems. MPC, a controller that utilizes a model of the process under control, has been particularly successful in fields such as chemical engineering, where the required sampling times are seconds or minutes long. However, our supervisor, Sina Nia Kosari (Ph.D. student in electrical engineering), sought to utilize MPC in robotic applications, where systems have faster dynamics. This requires much faster sampling rates in the order of milliseconds.

Run time of the MPC algorithm had to be improved to allow the use of such sampling rates. MPC aims to find the control input that minimizes the difference between the desired and actual response in a given optimization horizon (time interval over which an optimization problem is solved). The rate-limiting step of MPC is finding the input that minimizes the system's error in response- based on the specified model relating system input and output. This is done using numerical optimization software packages. After compiling a list of appropriate open source software packages, Jack and I installed HOPSPACK, NOMAD, and ACADO and used them to solve basic optimization problems, modifying portions of the code when necessary. We were able to achieve solution times in the millisecond time scale. Upon completing my involvement in this project, further testing was to be done to examine whether these solution times remained low when the complexity of the optimization problem is increased.

Applying MPC to robotic surgery requires an accurate model of intra-abdominal tissue. My capstone project builds on the mathematics and programming skills I have learned from my past work and provide the model that is required to advance the lab's application of MPC in surgical robotics.

I have also instrumented a Fundamentals of Laparoscopic Surgery (FLS) pegboard to record when the operator's left or right tool makes contact with the metal pegs, which is a sign of poor surgical performance. Previously, when either of the tools made contact with a metal peg, an LED powered by a small battery would light up to alert the test supervisor. These contacts would be tallied and accounted for in the overall performance score for the test. My improvement utilized a Phidgets microcontroller (USB powered) to record instances of tool-peg contacts (with a time stamp and a variable to indicate whether the right or left tool made contact) and to optionally drive a series of LEDs to alert the operator that they have made a mistake.

The microcontroller programming skills, in addition to those that I acquired by taking EE 472 (microcomputer systems), have greatly eased the learning curve in writing the Make Controller firmware for my project. Learned knowledge of circuits, such as the debouncing

circuits used to prevent multiple hit registrations per tool-peg contact, have also proved to be useful throughout the course of my current project.

Outstanding Technical Issues at the Onset of the Project

At the onset of the project, it was unclear what actuator would be most suitable for my project. While voice coils seemed promising, their single quantity prices were undetermined. Solenoids were not a viable alternative because of their high degree of nonlinearity. Professor Hannaford proposed hard drive voice coils as a potential option, but it was not clear at the start of the project how these would be used to create the linear motion necessary for the device.

At the time of my proposal I was still considering several sensors for measuring tissue displacement including linear variable displacement transformers, analogue Hall Effect sensors, and optical encoders with linear scales. Prices, frequency responses, appropriate linear ranges, needed to be investigated further before choosing which to use.

The overall mechanical design of the device would be very different depending on the type of actuator and displacement sensor chosen. Therefore, at the start of the project it was unclear what other components would be necessary to facilitate linear motion of the indenter and coupling of the sensor to its displacement. I knew that after choosing the actuator and sensor, there would have to be a significant amount of time spent coming up with a working overall design.

It was also not clear to me at the time at the onset of the project how I would drive the voice coil and collect data. A DAQ was a potential option, but would not be easy to incorporate with existing systems in the Biorobotics lab. The lab also uses a custom USB board for reading encoder values and driving various system components. However, it was clear that writing the firmware for this device and using it to read analog values could potentially be inconvenient. Other options included microcontrollers such as the Make Controller and devices made by a company called Phidgets.

Since I did not know what kind of device I was going be using for data acquisition and driving the voice coil, it was not clear how the data would be transmitted to the host PC.

DAQs and the BRL USB board would utilize serial data transmission. However, microcontrollers have several different options that needed to be investigated such as Xbee, TCP, UDP, and serial data transmission. It was unclear to me at the time which would be the most appropriate.

Regardless of the choice of device, driving the voice coil also presented a potential problem. Outputs on the microcontroller are current limited, so cannot source the amount of current required to drive the voice coil. I did not know how this issue was going to be resolved, although I did know that amplification of the current provided by the microcontroller would be required.

An additional outstanding technical issue was how tissue-indented contact would be detected to set the zero point for displacement measurements. This is important for accurate measurement of displacement, but because I was busy working on other design elements, this problem had still yet to be addressed.

Another issue with that was unresolved at the time was which method was going to be used for online data analysis. Options included recursive least squares techniques, extended Kalman filters, and unscented Kalman filters. It was not clear which I would use or how they would each be implemented in my project.

Design of Tools, Devices, and Experiments

Overview of Design and Research as Proposed in BIOEN 401

In BIOEN 401, I proposed that a linear voice coil actuator [31] would be used to apply a known force to soft tissue. A voice coil actuator was initially chosen because they are precise and their lack of gears or cables in these devices also suggests that they will likely have lower friction than the alternative actuating devices, which would help to maintain predictable output values [21].

Previous devices, such as those used in the studies by De *et al.* and Rosen *et al.* have used encoders to track the position of the driving motors [4, 23]. At the time of my proposal I was still considering several sensors for measuring tissue displacement including linear

variable displacement transformers, analogue Hall Effect sensors, and optical encoders with linear scales [32]. Figure 7 shows a general design layout for my proposed device.

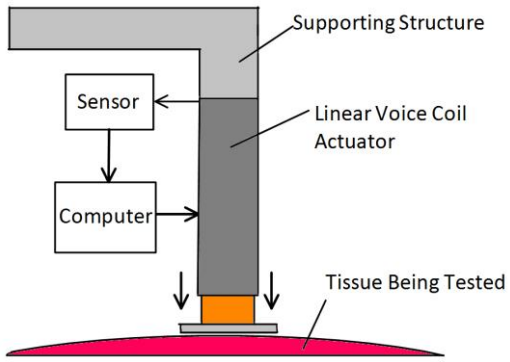

Figure 7: Diagram of device and system design. The linear voice coil actuator would respond according to the input current magnitude and compresses the tissue below. A sensor would measure displacement data, which would then sent to a computer for storage and processing. The software running on the computer would display information, store data, make calculations based on past and incoming data, and drive the voice coil actuator. Actuator trajectory would depend on the established testing protocol (sinusoidal force application, step force application, *etc.*).

Device calibration after assembly would provide the relationship between input current and force output. Protocol for calibration would vary depending on the chosen hardware, but I planned to use methods similar to those described in the study by Roan [22].

To validate device behavior, I planned to perform initial experiments on store bought meat. Once any needed refinements had been made and a working protocol was developed, I would perform experiments on *in vitro* porcine liver to determine which of a number of the available mathematical models for soft tissue described the data most with the best ratio of accuracy to computational cost. Once a finalized protocol was established, *in vivo* tests would be performed on porcine liver through the UW surgical pig lab using online data analysis.

Overview of Revised Design Process

Initial research on linear voice coils revealed that their cost was prohibitive, with quotes of $900 or more when purchased commercially in single quantities. Professor Hannaford pointed out that old hard drives are a source of rotating voice coil actuators. However, because these voice coils are rotational and not linear, the motion must be linearized to

perform the necessary actuation. It was decided that the best way to do this was to use a pulley attached to the hard drive to move the tissue indenter linearly.

The resulting tissue displacement is measured using a Linear Variable Differential Transformer (LVDT). This sensor was chosen because they have a very high resolution, high mechanical reliability, low friction, and very little temperature or humidity sensitivity.

In order to couple the motion of the indenter, the movement of the core of the LVDT, and the rotational motion of the hard drive actuator, the design shown in Figure 8 illustrates the design that I modeled in Solidworks to accomplish this.

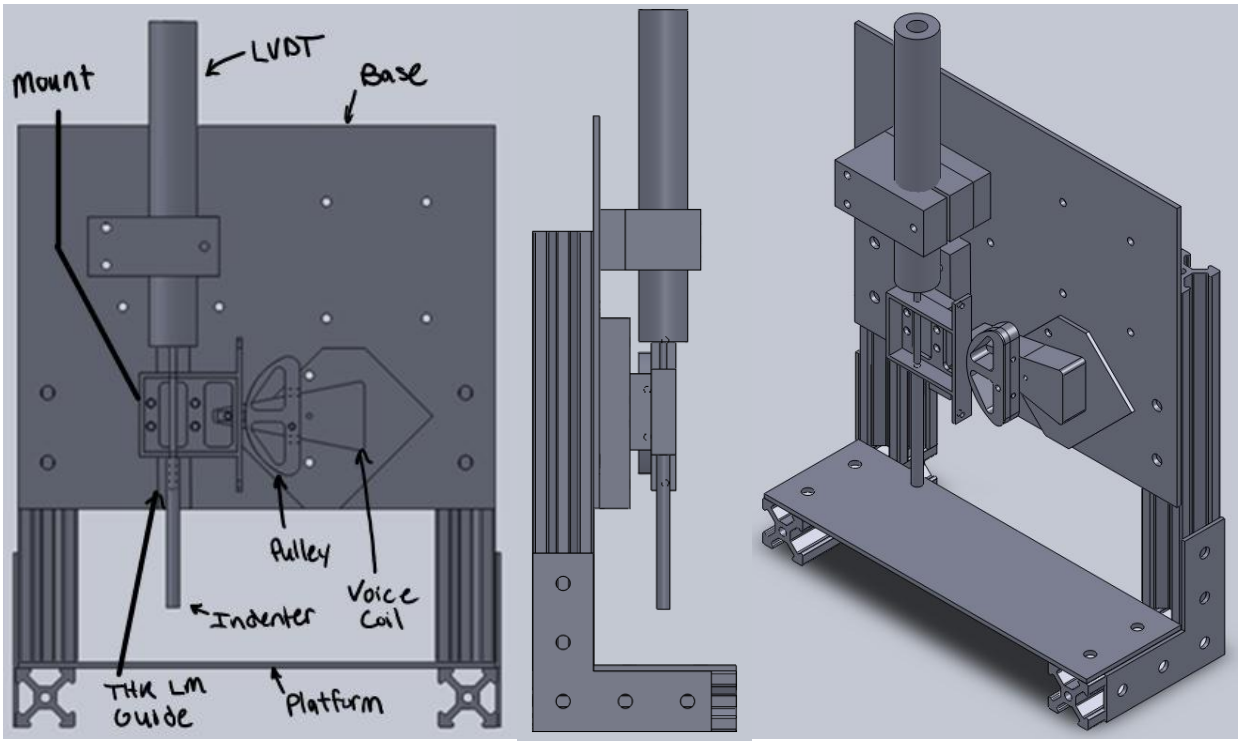

Figure 8: Front, left, and isometric views (left, middle, and right respectively) of my revised design.

The hard drive voice coil rotates in response to input current from an h-bridge controlled with pulse width modulation from a microcontroller. This moves the indenter upwards or downwards to compress the tissue, which is placed on the adjustable platform. Data is recorded on the microcontroller and sent to a host PC *via* network for processing and analysis.

Materials and Methods

Device Design, Fabrication, and Assembly

The voice coil actuator was salvaged from a Maxtor hard drive and excess case material was cut away using a hacksaw and Dremel. The pulley, indenter, mount, platform, and base were designed in Solidworks and then sent to Warren Tools and Development and Prunella Machine to be made out of non-anodized aluminum. CAD drawings for all custom parts can be found in the supplementary materials (will be made available in the coming weeks – details on how to access will be provided once completed).

Arduino Development

All firmware files for the various calibration protocols and experimental protocols will be made available in the supplementary materials. Rosserial, a Robotic Operating System (ROS) package has recently been made compatible with the Arduino platform. Therefore, I have made my device ROS compatible, so that all data collection and transmission can be performed utilizing the powerful built-in capabilities of ROS. More information on ROS can be found at www.ros.org. Instructions on how to operate my device and how to properly utilize the developed Arduino firmware files will be provided as supplementary materials.

Position Sensor Calibration

Although the LVDT position sensor comes with a factory calibration data sheet, the relationship between sensor output and displacement must be determined due to the fact that the sensor core alignment with the sensor body must be verified and that the output voltage gains have been adjusted to fit within the bounds of the Arduino analog input range of 0 to 5V.

1mm metal disks from the salvaged Maxtor hard drive (thickness verified with a micrometer) and 4mm 80:20 mounting brackets (thickness verified with a micrometer) were stacked in 1mm increments underneath the tool tip. This created 1mm increments in core displacement. By recording the sensor readings at each increment, a relationship between sensor output and core displacement can be established using a simple linear regression. Detailed calibration instructions, necessary Matlab files, and Arduino firmware files will be provided as supplementary materials.

Motor Calibration

Detailed calibration instructions, necessary Matlab files, and Arduino firmware files will be provided as supplementary materials. Note that in protocols requiring the ATI Nano17 force sensor, the force sensor was allowed to reach a steady state by warming up for approximately half an hour to avoid sensor drift and was tared before each trial.

Force vs. Current Calibration

The first calibration performed was a calibration to relate current input to the motor to force output of the motor. Force was measured using an ATI Nano17 force sensor (borrowed from Lee White for the calibration). Average current through the coil was measured by placing a 1 ohm resistor in series with the motor and then putting the voltage over the resistor through a passive low pass filter, a differential amplifier, an absolute value circuit, and a non-inverting amplifier. Note that the absolute value circuit is necessary because the control of the motor is bidirectional, meaning that the sign of the voltage reading across the resistor may be positive or negative. A rectifier is not appropriate in this case due to the fact that the loss across the rectifier is not constant. Absolute value circuits do not have this problem. A schematic of the device electronics will be provided as supplementary material.

Forces from 0.2N to 3.3N were applied in a ramp pattern by linearly varying the PWM duty cycle of the h-bridge input signals. A Matlab script was made to simultaneously read measurements from the force sensor and the current feedback circuit readings from the Arduino. A simple linear regression was applied to the collected data. The position of the indenter was recorded for later use.

Force vs. Position Calibration

It was also noticed that the force output of the motor for a given current value varies depending on the position of the motor due to variation in the magnetic field of the magnetic plates in the motor at the edges. In order to obtain this relationship, a constant current was applied to the motor and a force reading was taken at various motor positions by stacking 1mm and 4mm metal plates underneath the force sensor in order to fix the motor at the given position. Note that each force reading was recorded as the difference between the reading when applying the constant force and the weight of the device itself

(.7537 N). The reason for this is that the weight of the device itself does not change with motor position, only the force applied by the motor does. This curve can be normalized to the output force reading at the position the initial force vs. current calibration was performed to obtain a correction factor that can be used to account for the position of the motor in the overall motor calibration.

Calibration Validation

In order to test the combined calibration for the motor, a sinusoidal force trajectory (sum of 5 equally weighted sine waves of was applied to the motor in .07, .13, .35, 1.37, and .47 Hz). If the calibration is correct, the estimated force and the force measured by the force sensor should match with a low degree of error. Note that the position of the device was allowed to vary throughout this experiment by placing a piece of foam between the indenter and the force sensor. Detailed calibration instructions, necessary Matlab files, and Arduino firmware files will be provided as supplementary materials.

Variation of Measured Device Weight

Another potential concern with motor calibration is that the weight of the device had the potential to change with motor position. This was not initially obvious, and is a subtle point. Figure 9 shows a close up view of the mechanism used to linearize the motion of the device.

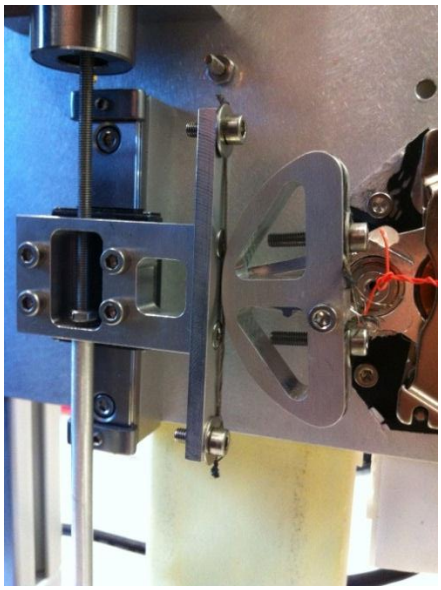

Figure 9: Close up view of the mechanism used to linearize the rotational motion of the voice coil

The portion of the mechanism in the left portion of Figure 9 (the portion mounted to the sliding rail) always has its center of mass in the same position relative to the indenter. However, the portion on the right (the voice coil arm and the pulley) undergoes rotation during operation. This causes the location of its center of mass to shift towards the axis of rotation as the motor rotates up or down from the center position. A test was performed that was identical to the calibration experiment used to find the relationship between the motor position and output force, except the motor was not turned on. Therefore, the weight of the device would be measured at various motor positions.

Simulations and Initial UFK Tests

Device Dynamics

The Unscented Kalman Filter implementation provides us with a method of simultaneously estimating the states and parameters of a system. In carrying out this analysis, it is important to recognize that the total system dynamics will be that of both the device itself as well as the tissue being studied. While we could have the Kalman filter perform an estimate on the both the device and the tissue, we can take advantage of the fact that the device properties should remain the same. Therefore, the following procedure can be used.

First, we can model the device as a mass with viscous friction term dependent on the velocity: $F_{motor} = m\ddot{x} + b\dot{x}$, where x is the position of the device. The mass of the device was measured, meaning that estimation of both the parameter b and the states, position and velocity, can be performed. The first step toward obtaining accurate results with our Kalman filter implementation is to obtain accurate estimation results with simulation data. This system was simulated in Simulink with a b value of 750 and an applied force input in the form of a 1Hz sine wave at a sample rate of 1000Hz for 60 seconds. After altering the Kalman filter implementation previously written by graduate student Sina Nia Kosari for the purposes of this particular estimation problem, the Kalman filter first state covariance matrix and noise covariance matrix were adjusted until accurate estimations of the position (match the simulation) were produced. In theory, a low error in the estimation of the states should lead to a low error in the estimation of the viscous friction term.

Combined Tissue-Device Dynamics

Having identified the viscous friction term and measured the mass, a combined model for the tissue-device system can be written. In order to do this, the equations for the dynamics of the tissue alone must be written. The most promising existing models for soft tissue dynamics (based on prior performance in literature) are:

a) Kelvin-Voigt: $F_{contact} = a + kx + b\dot{x}$

b) Mass-damper-spring: $F_{contact} = a + kx + b\dot{x} + m\ddot{x}$

c) Hunt-Crossley: $F_{contact} = a + kx^n + \lambda x^n \dot{x}$

Where $x, \dot{x}, and\ \ddot{x}$ are position, velocity, and acceleration respectively. However, the dynamic tissue model and the dynamic device model must be combined.

In order to combine the device and tissue models, we make the assumption that the states of the indenter surface and the tissue surface are the same. This allows us to write the equation $F_{motor} - F_{contact} = m\ddot{x} + b\dot{x}$. The combined device-tissue models are:

a) Kelvin-Voigt: $F_{motor} = m_{device}\ddot{x} + (b_{device} + b_{tissue})\dot{x} + kx + a$

b) Mass-damper-spring: $F_{motor} = (m_{device} + m_{tissue})\ddot{x} + (b_{device} + b_{tissue})\dot{x} + kx + a$

c) Hunt-Crossley: $F_{motor} = (b_{tissue} + \lambda x^n)\dot{x} + kx^n + a$

Using these combined models in conjunction with the UKF, we can estimate the unknown states and parameters in the above models. Since F_{motor} and position (from which we can derive acceleration and velocity), we can ensure accurate results by comparing estimated position and velocity to the measured position and its derivative, as well as the estimated motor force, based on the above equation with estimated values substituted in, to the measured motor force. Position and velocity estimates should be relatively close to the measured values, and the comparison of motor force estimate to measured motor force will provide insight as to how well the parameterized model describes the system dynamics.

An initial simulation in Simulink was performed to ensure that the Kalman filter performed as expected. Results are not included in the report, but they indicate that the Kalman filter can be adjusted to obtain accurate results. All necessary C/C++ and Matlab files for the UKF implementation and analysis of results will be provided as supplementary materials.

UKF Results Based on Collected Data

Device Dynamics

Once proper behavior was verified, the device applied a force to counter its weight (allows it to be positioned), allowed to reach a stopping position, and then driven with the same force trajectory as in the Simulink simulation, and the displacement from the initial position and force were recorded at 126 Hz. The Unscented Kalman filter was used to identify the b term as before. In order to test the accuracy of this estimate, we can fix the b term and estimate the states on a new set of data.

Phantom Tissue Dynamics

Simulab complex tissue model phantom tissue (Part TSC-10) was placed underneath the indenter. The device applied a force to counter its weight (allows it to be positioned) and the indenter was positioned such that its surface was just in contact with the tissue surface. Force was then applied to the tissue following an equally weighted sum of five sine waves of 0.7, 1.0, 2.4, 3.3, and 4.2 Hz. Position and force were recorded throughout the trial at 126 Hz. Data was analyzed utilizing the UKF with each combined device-tissue dynamic model.

In Vivo Tissue Dynamics

Due to delays in the IACUC approval process and proper calibration of the device, I have not completed the *in vivo* experiments at this time. However, I am scheduled to perform these experiments on June 13th with the help of Dr. Thomas Lendvay (Seattle Children's Hospital) at the Center for Video Endoscopic Surgery at the University of Washington Medical Center. Due to the presence of respiration in *in vivo* tissues, frequencies above 1 Hz will be used in applying forces to the tissue to avoid conflict with the respiratory rates (well under 1 Hz, especially under anesthesia). This will allow the respiration artifact in the data to be filtered out of the signal. These data files, Kalman filter analysis, and any other supplementary materials will be made available once the experiments are completed. It should be noted that my capstone advisors and I have agreed to this arrangement.

Costs

Table **1** enumerates the cost of all the items that have been purchased for the purpose of this project.

Table 1: Enumeration of project expenses

Item	Unit Price (Dollars)	Quantity	Overall Price
Measurement Specialties HR500 AC LVDT	162.00	1	162.00
Measurement Specialties HR500 AC LVDT Mounting Block	34.00	1	34.00
M3x0.5-6H6 Connecting Rod for Measurement Specialties HR500 AC LVDT	28.00	1	28.00
Measurement Specialties LVM110 AC LVDT Signal Conditioning Unit	174.00	1	174.00
Texas Instruments SN754410NE	2.14	4	8.56
Custom Machined Parts from Prunella Machine	683.00	1	683.00
Custom Machined Parts from Warren Tool and Development	431.00	1	431.00
Solderless Breadboard	6.00	1	6.00
THK Linear Motion Guide (RSR7WZUU+80LM)	55.00	1	55
Arduino Nano	40.00	1	40.00
Passive Circuit Components from lab supplies	10.00	1	10.00
Simulab Complex Tissue Model	75.00	1 (Not paid for, for purposes of this project)	0.00
PCB Board	30.00		30.00
Project Case from Sparkfun	9.00		9.00
Parts for PCB Circuit	15.00		15.00
In Vivo Experimental Costs	Undetermined		
		TOTAL	1685.56

It should be noted that since the voice coil actuator used in this project was salvaged from a non-functional hard drive, it did not cost any money to obtain. The only costs associated with the *in vivo* experiments are for paying the vet techs for 2-3 hours of extra time. Since the animals are not obtained solely for the purposes of my experiments, but rather for surgical training in the Center for Videoendoscopic Surgery, animal costs are avoided.

Details of Design Process and Statistical Basis for Experiments

Design Process

Initial research on linear voice coils revealed that their cost was prohibitive, with quotes of $900 or more when purchased in single quantities. Solenoids were considered as a cheaper

alternative, but ultimately proved not to be applicable due to their high degree of non-linearity. Professor Hannaford pointed out that old hard drives are a source of rotating voice coil actuators. A previous study in the lab has shown that these actuators produce a relatively linear input current to output torque ratio and of high quality [33]. However, because these voice coils are rotational and not linear, the motion must be linearized to perform the necessary actuation. It was decided that the best way to do this was to use a pulley attached to the hard drive to move the tissue indenter linearly.

The resulting tissue displacement is measured using a Linear Variable Differential Transformer (LVDT) position sensor. LVDT outputs are proportional to the position of the core of the LVDT within the coils. This sensor was chosen because of its high resolution, high mechanical reliability, no friction, and little temperature or humidity sensitivity.

The design in Figure 8 illustrates that the motion of the indenter, the movement of the LVDT core, and the rotational motion of the hard drive actuator are coupled to enable positon measurement. The hard drive voice coil rotates in response to input current. In this design the LVDT core is connected *via* a threaded rod to a custom mounting piece, which also coupled via short cables to the pulley. The custom piece labeled as "mount" is mounted to the base by a THK linear motion guide (RSR7WZUU+80LM), which allows the whole unit to move in the vertical direction. It should be noted that the indenter cap is removable, allowing for use of different shapes, or alternate studies in surgical tasks such as needle insertion and retraction. The tissue sits on the adjustable platform and is compressed by the indenter. The base also has holes for mounting additional circuitry, the LVDT signal conditioner, and a microcontroller. Any custom parts in this design were ordered local machinists. The adjustable platform utilizes premade 80/20. CAD drawings of all custom parts are made available in the supplementary materials.

The voice coil is controlled using an h-bridge and pulse width modulation (PWM). The h-bridge applies a load voltage to the voice coil with up to 1A continuous current and 2A peak current. It also has a logic input to control the application of this voltage across the motor leads. Using PWM, this logic input can be used to vary the torque output of the voice coil.

PWM is provided by an Arduino Nano. This microcontroller is also used for initial preprocessing according to the calibration to record position measurements. An additional circuit to measure the average current across the motor was constructed because motor heating was observed to produce variation in the resistance of the voice coil, leading to a drop in current for a given applied voltage. While this problem could be solved using a constant current source, the least expensive solution was to add a feedback circuit that measures average current across the motor as the PWM duty cycle is varied. The circuit diagrams for all electronics will be provided in the supplementary materials.

Statistical Basis for Experiments

Device calibration experiments were performed using 360 (60 seconds at 6 Hz) data points in order to ensure a high enough sample population. R^2 values are used to evaluate the quality of the fit, and standard deviations of the data were taken to provide error bars. Average and maximum errors are reported for these experiments. For validation, a completely new data set was used to evaluate the calibration.

In the phantom tissue tests, the average errors and parameter values reported are taken as an average of the last 1000 points in the data set. Results of the adjustments made to the Kalman filter settings were evaluated by collecting a separate data set on the same location on the phantom tissue under approximately the same experimental conditions. Once the Kalman filter is performing as expected, a t-test can be used to compare the results from trials taken in the same location.

In the *In vivo* tests, we are currently limited to one animal. As we are simply trying to demonstrate that the models can be parameterized for for *in vivo* porcine abdominal organs, this does not impact the statistical relevance of the results. The number of trials will be as high as time allows in the 2-3 hour session. At least three trials will be taken in every tested location, so that results from each data set can be compared after Kalman filter tuning. Since the values from these trials are based on 1000 points or more each, appropriate statistical methods, such as a t-test can be used to compare the three trials.

Results

Gantt Chart

My original Gantt chart is shown in Figure 10.

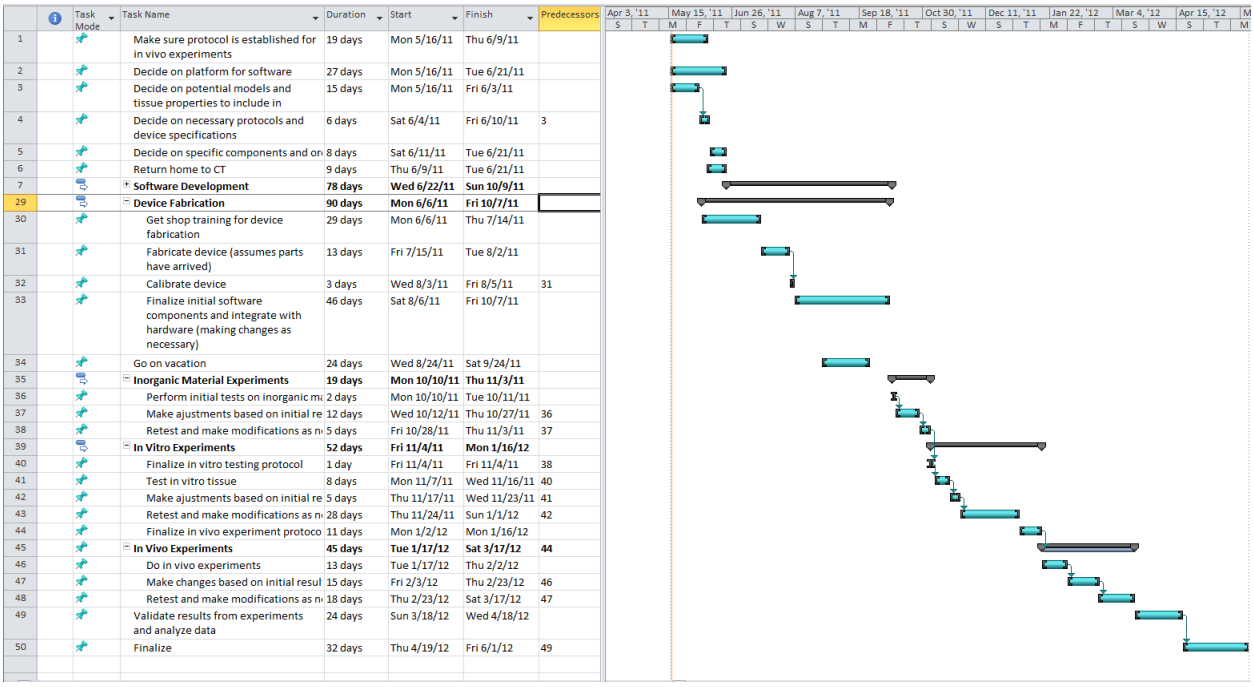

	Task Mode	Task Name	Duration	Start	Finish	Predecessors
1		Make sure protocol is established for in vivo experiments	19 days	Mon 5/16/11	Thu 6/9/11	
2		Decide on platform for software	27 days	Mon 5/16/11	Tue 6/21/11	
3		Decide on potential models and tissue properties to include in	15 days	Mon 5/16/11	Fri 6/3/11	
4		Decide on necessary protocols and device specifications	6 days	Sat 6/4/11	Fri 6/10/11	3
5		Decide on specific components and on	8 days	Sat 6/11/11	Tue 6/21/11	
6		Return home to CT	9 days	Thu 6/9/11	Tue 6/21/11	
7		**Software Development**	**78 days**	**Wed 6/22/11**	**Sun 10/9/11**	
29		**Device Fabrication**	**90 days**	**Mon 6/6/11**	**Fri 10/7/11**	
30		Get shop training for device fabrication	29 days	Mon 6/6/11	Thu 7/14/11	
31		Fabricate device (assumes parts have arrived)	13 days	Fri 7/15/11	Tue 8/2/11	
32		Calibrate device	3 days	Wed 8/3/11	Fri 8/5/11	31
33		Finalize initial software components and integrate with hardware (making changes as necessary)	46 days	Sat 8/6/11	Fri 10/7/11	
34		Go on vacation	24 days	Wed 8/24/11	Sat 9/24/11	
35		**Inorganic Material Experiments**	**19 days**	**Mon 10/10/11**	**Thu 11/3/11**	
36		Perform initial tests on inorganic ma	2 days	Mon 10/10/11	Tue 10/11/11	
37		Make ajustments based on initial re	12 days	Wed 10/12/11	Thu 10/27/11	36
38		Retest and make modifications as n	5 days	Fri 10/28/11	Thu 11/3/11	37
39		**In Vitro Experiments**	**52 days**	**Fri 11/4/11**	**Mon 1/16/12**	
40		Finalize in vitro testing protocol	1 day	Fri 11/4/11	Fri 11/4/11	38
41		Test in vitro tissue	8 days	Mon 11/7/11	Wed 11/16/11	40
42		Make ajustments based on initial re	5 days	Thu 11/17/11	Wed 11/23/11	41
43		Retest and make modifications as n	28 days	Thu 11/24/11	Sun 1/1/12	42
44		Finalize in vivo experiment protoco	11 days	Mon 1/2/12	Mon 1/16/12	
45		**In Vivo Experiments**	**45 days**	**Tue 1/17/12**	**Sat 3/17/12**	**44**
46		Do in vivo experiments	13 days	Tue 1/17/12	Thu 2/2/12	
47		Make changes based on initial resul	15 days	Fri 2/3/12	Thu 2/23/12	46
48		Retest and make modifications as n	18 days	Thu 2/23/12	Sat 3/17/12	47
49		Validate results from experiments and analyze data	24 days	Sun 3/18/12	Wed 4/18/12	
50		Finalize	32 days	Thu 4/19/12	Fri 6/1/12	49

Figure 10: Original Gantt chart

Due to some initial misconceptions about the project and a lack of initial agreement on the approach to be used for the mechanical design, the finalizing of the design did not occur until much later than anticipated. Most of summer quarter was spent choosing components and drafting designs in CAD. All the necessary parts to build the device were not obtained until the end of fall quarter. My winter quarter progress quickened significantly as I was able to complete construction of the device and basic electrical design implementation within a few weeks. Problems with the calibration procedure required additional components to be added and the microcontroller had to be changed. This resulted in significant delays, meaning that the calibration was not completed until the past few weeks. In parallel I readied the Kalman filter implementation for data analysis. Again, this is much later than my initial Gantt chart estimated. Due to the delay in the design and calibration, the *in vivo* experiments have been pushed back as well. Overall, my original Gantt chart is a very poor representation of how my project schedule went. However, I believe that I still

managed my time quite well throughout the entire process. I believe that the discrepancies can be attributed to the fact that I had very little previous experience in planning such an extensive project. This has been a valuable experience in illustrating how almost every aspect of a project can take longer than anticipated.

Mechanical Design

The initial CAD designs were sent to Prunella Machine and Warren Tool and Development for manufacturing. The parts returned were excellent and met the specifications extremely well. In constructing the device, all the parts fit together as intended, with no major modifications. The steel cables used to attach the pulley exhibited no observable stretch for the range of forces applied by the motor. The wires to the leads of the voice coil were of very thin gage and were given adequate slack. This prevents the wires from impacting the forces applied by the motor. A picture of the finished device is shown in Figure 11. A video of the finished device in operation will be provided in the supplementary materials.

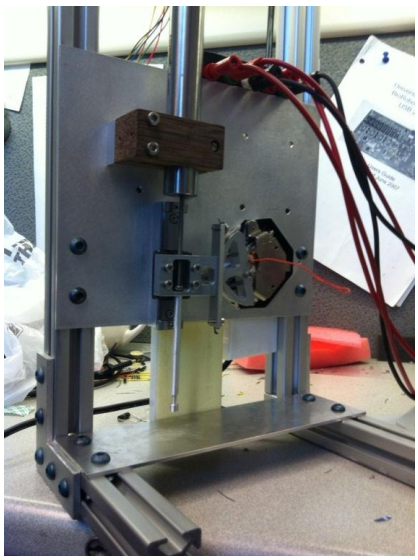

Figure 11: Finished construction of the mechanical portion of the device.

Electrical Design

The final electrical design for the device works as intended. The components include an h-bridge circuit to drive the voice coil motor, a second order low pass filter circuit and voltage divider to filter out some high frequency noise in the LVDT signal and bring the

voltage into the 0-5V range of the Arduino analog inputs, the signal conditioning unit provided with the LVDT, and a circuit to read the average current through the voice coil.

Another problem that was encountered throughout this process involved the Make Controller 2.0, the original microcontroller used in the design. During winter quarter, the website that houses all of the support information for the microcontroller went down indefinitely (we think they may be going out of business). For this reason, the firmware was transferred to an Arduino Nano 3.0 platform. This change was made relatively easy due to the strong support community and documentation provided on the Arduino website.

It also became clear in initial testing that the ground used for the motor power source and the current feedback/LVDT circuit would have to be separated. This is explained by the fact that the high current drawn by the motor is can cause the ground to be pulled up. Since this occurs at the PWM frequency, this resulted in a significant amount of noise in the LVDT and current readings. The ground used for each was separated to avoid this issue. The final electrical design is shown in the picture in Figure 12.

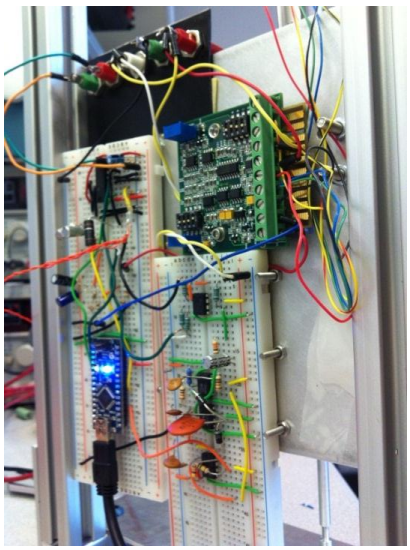

Figure 12: Final electrical design components

It should be noted that a PCB design was made for the initial design using EAGLE CAD. Unfortunately, this circuit did not include the current feedback components, and has since been redesigned. The conversion to PCB may result in changes in the calibration, so the PCB will be not installed until I am finished with my experiments. Since the signals do not

exhibit significant noise, it does not appear that there is any loss in signal integrity. A PCB design would be much less fragile and is much better permanent option. The circuit diagram of the electronics will be provided in the supplementary materials.

Position Sensor Calibration

The first step in the device calibration process was to verify that displacements in the LVDT core resulted in linear changes in the output voltage, and to determine the relationship between the output voltage and the displacement of the core (Figure 13).

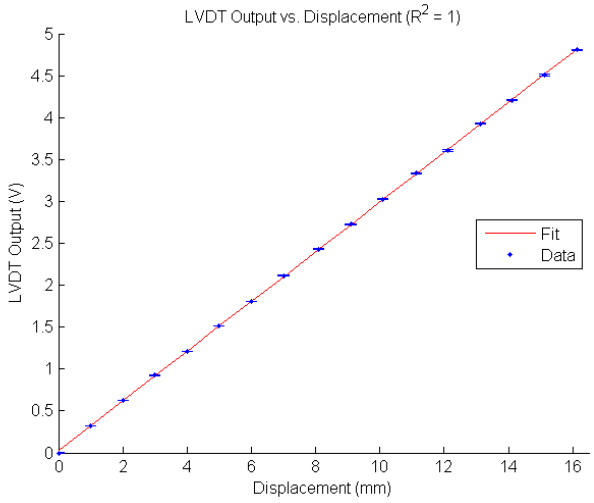

Figure 13: 1mm and 4mm plates (verified with a micrometer) were stacked underneath the device to produce precise displacements from 0 to 16 mm. The LVDT output was measured at each of these points and plotted against the displacement values. A linear fit was applied, resulting in $R^2 = 1$. Error bars in the plot represent one standard deviation in the sensor output reading in each direction.

These results indicate that then sensor behavior is reliable.

Motor Calibration

Force readings were taken at various current values in order to obtain a relationship between motor output force and average current. The results from this experiment are shown in Figure 14.

Force vs. Current Calibration

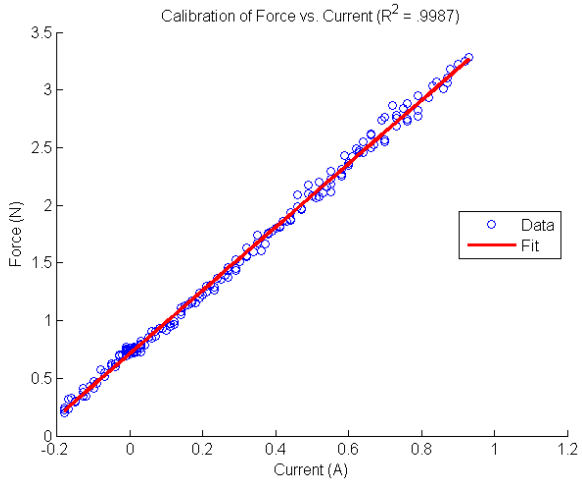

Figure 14: The duty cycle of the h-bridge logic input was varied linearly in order to travel between minimum (upward force of the motor approximately equal to weight of device) and maximum downward force. Current values are negative if the motor is lifting the device upwards to counter its weight. A linear fit was applied, yielding a R^2 value of 0.9987.

The high R^2 value indicates that this is a good fit. The position of the motor was recorded during this experiment for use in subsequent motor calibration steps.

Force vs. Position Calibration

The result of this experiment are shown Figure15.

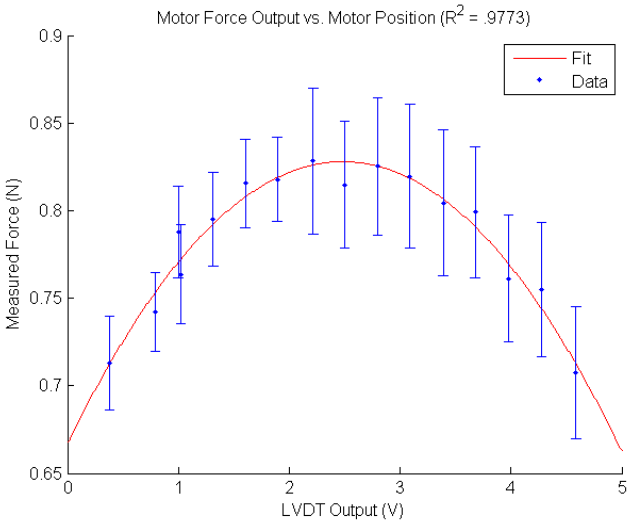

Figure15: The motor was set to a constant duty cycle and allowed to reach a steady current value. Using the force sensor, the force was measured at various motor positions. The weight of the device was then subtracted from the total force (as this does not change significantly with motor position). A quadratic fit was applied to the adjusted force vs. LVDT output data resulting in R^2 = 0.9773. Error bars represent one standard deviation in each direction.

The high R^2 value obtained using a quadratic fit implies that the fits the data well. However, there is a reasonable amount of noise in the data. Unfortunately, this appears to be variation in the force sensor reading. While the differences between the points here are statistically significant, a lower level of noise would be desirable. A better force sensor or perhaps a data collection setup that allows for higher sampling rates, and thus filtering, would potentially help to reduce noise.

Variation of Measured Device Weight

The experiment demonstrated no statistically significant difference in the readings at any of the motor positions. One possible reason for this is that the weight of the pulley and arm are very low with respect to the total mass and that their center of mass is likely close to the rotational axis of the voice coil. Due to the fact that the changes in weight are likely very small, the noise in the force sensor readings could mask some very small differences.

Motor Calibration Validation

The following two sets of results in Figure 16 and Figure 17 were obtained by performing this experiment in the upper and lower range of the motor respectively (ensures that the entire path of the motor is tested).

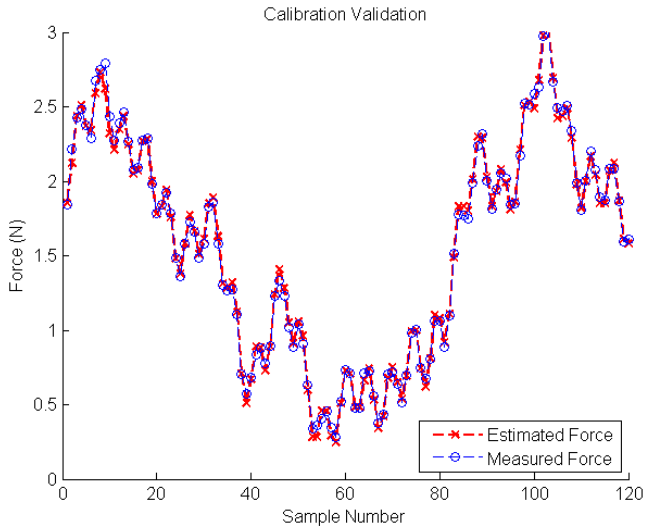

Figure 16: Results from the calibration experiment in the upper range of motor position. Note that the forces were applied in a sinusoidal trajectory with equally weighted components at 0.07, 0.13, 0.35, 1.37, and 0.47 Hz

The mean difference between the estimated force and the measured force is 0.034 N with a standard deviation of 0.028 N. The maximum error observed was 0.17 N in this experiment. Due to limitations in the data collection setup that collects data from the force sensor and the Arduino, a sampling rate of 7 Hz is used. The current setup is in Matlab, and may need to be translated to C in the future to obtain faster sampling rates.

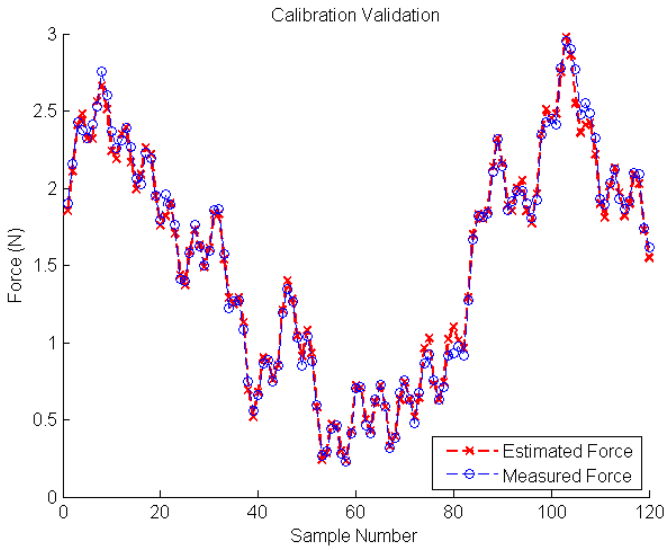

Figure 17: Results from the calibration experiment in the lower range of motor position. Note that the forces were applied in a sinusoidal trajectory with equally weighted components at 0.07, 0.13, 0.35, 1.37, and 0.47 Hz

As in the upper half of the trajectory, the average magnitude of the error is low: 0.0359 N with a standard deviation of 0.0322 N. The maximum error observed was 0.22 N.

Simulations and Initial UKF Tests

Device Dynamics

The results of this analysis are shown in Figures Figure 18, Figure 19, and Figure 20.

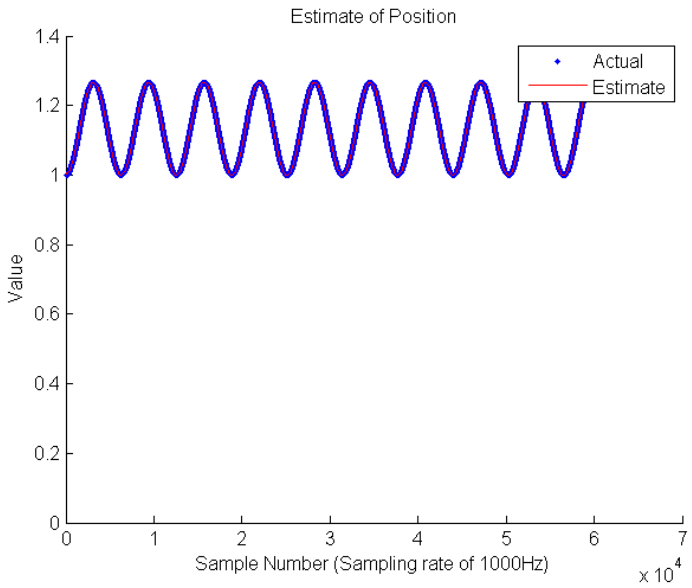

Figure 18: Estimate of the position and the actual position in the simulation data

The position estimation has an average error magnitude of 1.43e-6. This low error indicates that the estimate is very accurate for position.

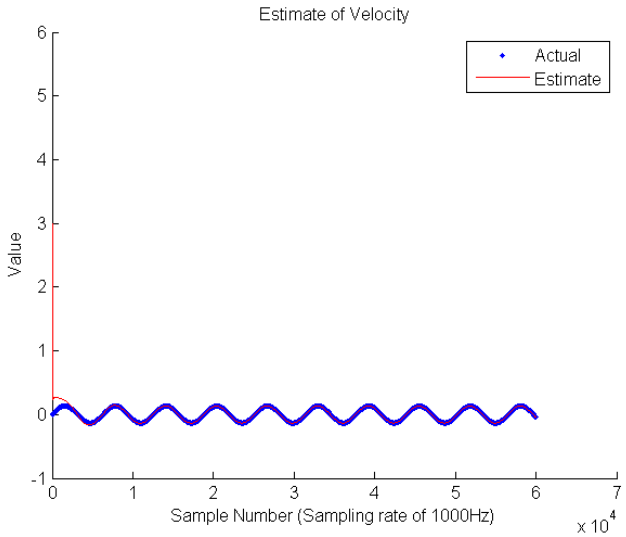

Figure 19: Estimate of velocity and actual velocity in the simulation

The average magnitude of the error after the first 10 seconds is 5.17e-4. It should also be noted that there is a spike in the estimation towards the beginning of the analysis. These results indicate that there may need to be further adjustments made to the covariance matrix to obtain more accurate results.

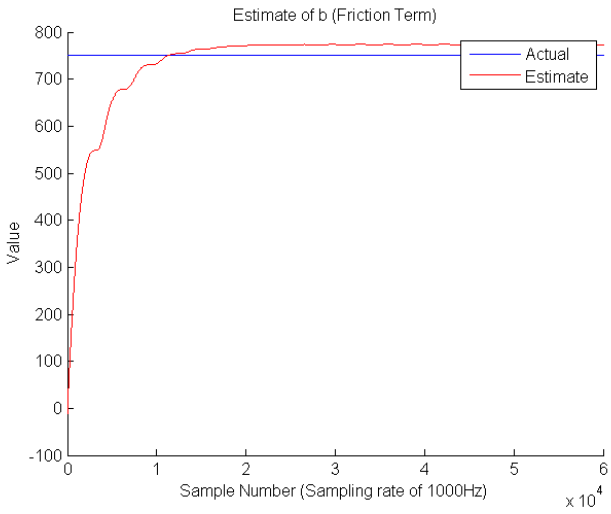

Figure 20: Estimation of the viscous friction term b and the simulation value

The steady state error in the estimation is 23.64, which represents a 3.15% error. While this is relatively low, it is possible that the analysis can be adjusted to obtain more accurate results. Another potential cause of this error is a lack of excitation in the system, which could be addressed by using an input force that is the sum of several different frequencies.

UKF Results Based on Collected Data

Device Dynamics

While data has been collected to quantify the device dynamics, the velocity state estimate still retains a large amount of error. Since this will be used to calculate the viscous friction term in the device dynamic model, it cannot be assumed that the friction term is correct until the velocity estimate is correct. Further efforts will be needed to refine the Kalman filter analysis before the device dynamics can be accurately quantified. An arbitrary value of 0.01 has been assigned to this term in the subsequent results, introducing a constant error term into b2 terms in the parameters identified in the models below.

Phantom Tissue Dynamics

Kelvin-Voight:

After tuning the Kalman filter based on the first data set, it was determined that the mean error in the position and velocity estimates were 0.13% and 450.3% respectively. Analyzing the second data set with these settings yielded mean error in the position and

velocity estimates of 0.14% and 479% respectively. The estimated motor force for the two data sets is plotted against the measured values in Figure 21 and Figure 22.

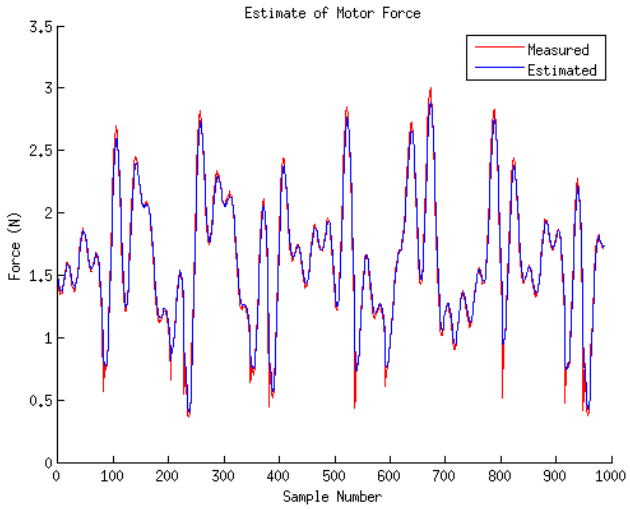

Figure 21: Plot of estimated and measured motor force for first data set

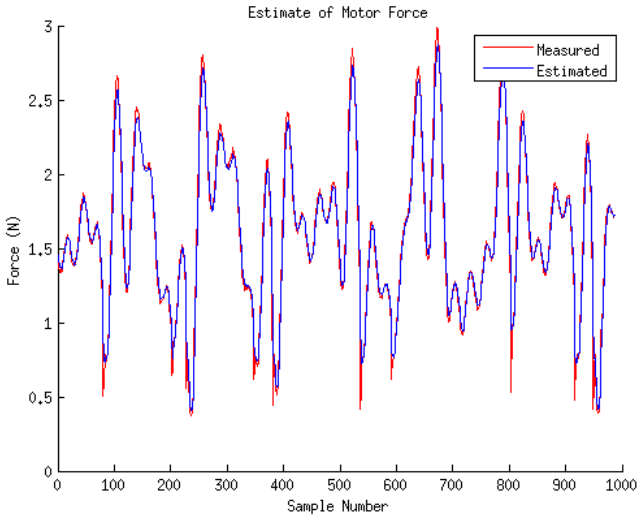

Figure 22: Plot of estimated and measured motor force for second data set

The mean error between the estimated and measured motor force is 3.92% and 3.86% in the first and second data sets respectively.

The parameters identified in these models are k = 230.11 and b2 = 24.01 in the first data set and k = 230.556 and b2 = 24.02 in the second data set.

Mass-Damper-Spring

After tuning the Kalman filter based on the first data set, it was determined that the mean error in the position and velocity estimates were 9.8E-4% and 363.7% respectively. Analyzing the second data set with these settings yielded mean error in the position and velocity estimates of 0.11% and 243.0% respectively. The estimated motor force for the two data sets is plotted against the measured values in Figure 23 and Figure 24.

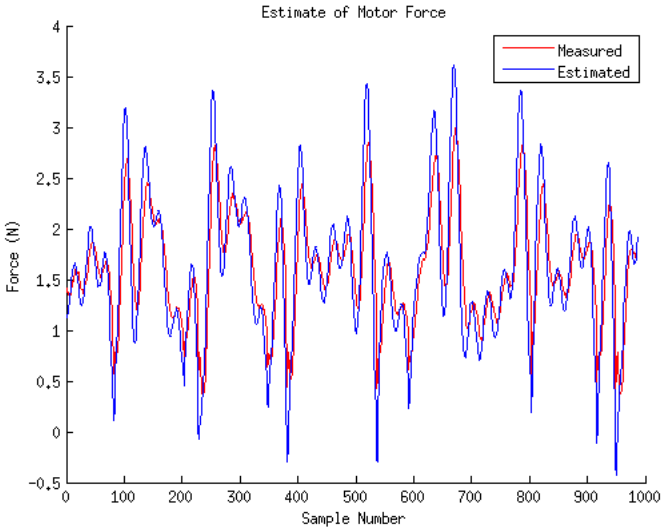

Figure 23: Plot of estimated and measured motor force for first data set

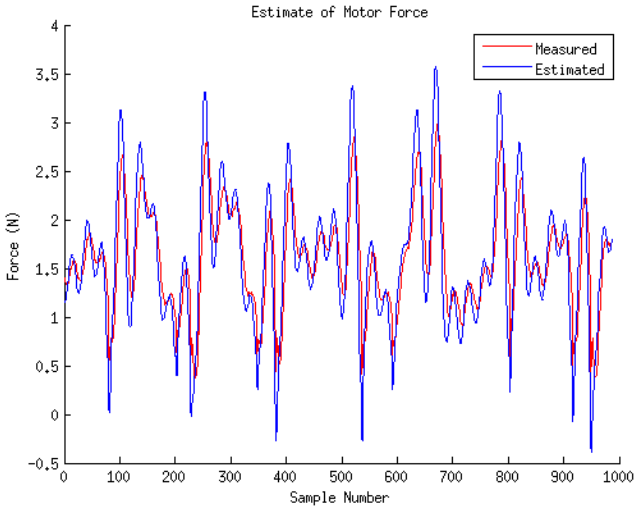

Figure 24: Plot of estimated and measured motor force for second data set

The mean error between the estimated and measured motor force is 20.19% and 19.91% in the first and second data sets respectively.

The parameters identified in these models are m2 = 3.0, k = 229.1, and b2 = 64.95 in the first data set and m2 = 3.0, k = 239.85, and b2 = 64.93 in the second data set.

Hunt Crossley

The Hunt Crossley model proved to be particularly sensitive to adjustments in the Kalman filter settings, and often fails to come to a solution entirely. Thus far, this model has not been able to be adjusted to provide state or motor force estimates that are at all close to the measured results. Therefore, the results will not be included here. Further adjustments will be needed to use this model and results will be provided as supplementary materials.

In Vivo Tissue Dynamics

Due to delays in the IACUC approval process and proper calibration of the device, I have not completed the *in vivo* experiments at this time. However, I am scheduled to perform these experiments on June 13th with the help of Dr. Thomas Lendvay (Seattle Children's Hospital) at the Center for Video Endoscopic Surgery at the University of Washington Medical Center. These data files, Kalman filter analysis, and any other supplementary materials will be made available once the experiments are completed. It should be noted that my capstone advisors and I have agreed to this arrangement.

Experimental/Design Decisions Made by the Student During Project

Throughout the course of the project there were several decisions that I made regarding experiments or design considerations.

Throughout the initial design phase, I chose to make several revisions to my initial design based on the cost of various parts and quotes on the custom parts that I had made for my project. I made the decision that I wanted to minimize use of any expensive components, while maintaining the robustness of the design.

During the initial calibration process, it became clear that the Make Controller 2.0 microcontroller, while otherwise robust, was not able to perform some of the floating point calculations required for calibration. In addition, the website that houses all of the support

information for the microcontroller has been down since winter quarter (we think they may be going out of business). For this reason, I made the decision to transfer the firmware to an Arduino Nano 3.0 platform. This platform will also make it very easy for future users of the device to alter the firmware due to the open source nature of Arduino and ROS.

In addition, it also became clear that the heating of the voice coil during operation was causing the calibration to become inaccurate due to changing resistance in the coil. I made the decision to add a current feedback circuit in order to improve the calibration.

Initially, I planned to automate contact detection with the tissue. This proved to be rather difficult to employ using only the position readings. I made the decision to instead provide an initial step in each experiment where the device is held in gravity compensated mode (force of the motor counters the weight of the device). The user can then set the position of the device such that it is just in contact with the tissue. The device is held in this position until the experiment is initiated, at which time the initial position is recorded for reference.

Lastly, my original idea was to enable a user to command forces to the motor during an experiment using a PID controller. However, this is not necessary for my experiments, and will only be used in future work. I have made the decision to omit this feature for the time being. Using a constant current power source is another potential option that would likely eliminate the need for PID control.

Analysis and Conclusions

Position Sensor Calibration

The results from the LVDT calibration indicate that there is a reliable relationship between its output voltage and the position of the device. The device was designed to place the core of the LVDT exactly in the center of the coil, and to ensure that the coil remained in the linear range of the device. Based on these results, it is clear that placement of the core within the coil is sufficiently accurate to maintain the linear behavior of the sensor. Furthermore, the low standard deviation of the sensor output measurements indicate that the reading is reliable and relatively noise free.

Motor Calibration

Results from the current to force calibration indicate that there is a strong linear relationship between the output force and the current through the device, as indicated by the R^2 value of 0.9987. The data show that there is some noise in the force measurement. Future efforts could seek to reduce noise to obtain lower bounds of error on the device.

The noise in the force sensor readings also poses a number of complications in the other steps of motor calibration. For example, this noise is apparent in the calibration of variation in the motor output force with position of the motor. The error bars in this calibration experiment overlap in many case (but not in others). Ideally, this noise would be reduced somewhat to reduce the variation in these measurements

Motor Calibration and Validation

Initial results for the overall calibration are promising. Average error is quite low and when calculated as a percentage error in estimated force represents an average of 3.5% and 3.7% in the upper and lower ranges respectively. One potential concern with this experiment is that when the device is in motion, the contact force may not be exactly equal the contact force. This potentially introduces some additional error into the results of this experiment. Given the noise in the force sensor readings, it is difficult to tell whether this error is a result of error in the calibration, or simply a product of the noise. Due to the nature of this experiment, the force measurements are single readings. In other experiments the noise in the force readings, assuming it is destructive, should not play a significant role because it will average out given the high number of samples.

Simulations and Initial UKF Tests

Device Dynamics

Initial simulation results with the Kalman filter are promising. The 3.15% error in the viscous friction parameter estimation also supports this claim. However, despite the relatively small errors, overall performance thus far is good. Another potential cause of the error is a lack of sufficient excitation in the system. A solution to this problem would be to use a force input that is the sum of three sinusoids of different frequencies.

UKF Results Based on Collected Data

Device Dynamics

While the simulation obtains relatively accurate results, usable results have not yet been obtained using the collected data. There are a number of items that should be examined as potential problems. The forces used in these experiments are very close to zero and of low magnitude. It is possible that the small non-linearity in the initial calibration data has resulted in overestimation and thus high percent error of the motor force in this range and magnitude. It is possible that a piecewise calibration curve could be used to account for the small non-linearity. It is also possible that the model is simply not an accurate representation of the device dynamics. An arbitrary value of 0.01 has been assigned to this term in the subsequent results, introducing a constant error term into b2 terms in the parameters identified in the models below. Further work should be done to determine if inclusion of factors such as static friction could improve the results. Lastly, as in the phantom tissue analysis, it is possible that the Kalman filter simply needs to be further adjusted. See the section below for suggestions on how this issue might be resolved.

Phantom Tissue Analysis

Error in the estimated motor force for each of the models examined is relatively low. However, due to the high amount of error in the velocity estimates, the performance of each model cannot be accurately evaluated. Error in the velocity propagates error into the parameter estimates, and this into the estimated motor force. Further refinements to the Kalman filter analysis will be needed before the results of these experiments can be commented on. One potential approach would be to use an implementation of the Robins-Monro algorithm, which can use stochastic variations to adaptively determine the appropriate covariance matrix of the Kalman filter. Similar problems have been observed in past work with the UKF implementation, so it is likely that they can be resolved given further refinement. Accurate viscous friction estimation for the device will also have to be ensured in order to accurately determine the b2 terms in each of the models.

In Vivo *Tissue Dynamics*

Due to delays in the IACUC approval process and proper calibration of the device, I have not completed the *in vivo* experiments at this time. However, I am scheduled to perform these experiments on June 13th with the help of Dr. Thomas Lendvay (Seattle Children's

Hospital) at the Center for Video Endoscopic Surgery at the University of Washington Medical Center. These data files, Kalman filter analysis, and any other supplementary materials will be made available once the experiments are completed. It should be noted that my capstone advisors and I have agreed to this arrangement.

Suggestions for Future Work

There are a number of additions to this device that should be implemented in the future. Since the weight of the device is included in the calibration, the device is currently limited to the vertical pose. A potential add-on that could enable the device to be used in any orientation would be an accelerometer to sense gravity. A potential improvement to the calibration procedure would be to write the program that collects the force sensor data in C to enable faster sampling rates.

By its conclusion, this project will have employed online mechanical property estimation on *in vivo* tissues. Since the utility of this device is so general, there are many potential applications that should be explored. As discussed in the project motivation, the mechanical properties estimated by this device could potentially be utilized in model-predictive control of surgical grasping. Graduate student Sina Nia Kosari will use this device to perform initial tests on whether or not this is possible, and what benefits it provides. Simultaneous control of the force/position of the device and state and parameter estimation will require adjustment to the Kalman filter analysis. Also, as this device is only for proof of concept, the features of this device, or something similar, would have to be incorporated into a surgical tool in order to reach the clinic.

Due to the fact that the tool tip of the indenter is interchangeable, studies can be done with indenters of various sizes and shapes. There has been research to suggest that the shape of surgical tools can influence the amount of damage that they cause, and this device could allow for further research in this area. This data would potentially be useful in partial automation of surgery and could be easily obtained.

Lastly, there is a potential application of this device in haptic enabled devices. Current research in my laboratory is focusing on haptic enabled equipment for astronauts that compensate for the mechanical impedance of the interface point with the human body. This

application would require knowledge of the dynamic mechanical properties. Using this device, one could ascertain the mechanical properties, enabling impedance compensation for these haptic devices.

Additional Research Projects and Presentations

Haptic Glove Project

I had the opportunity to take EE 589: Haptic Enabled Devices, which was taught by my graduate student mentor, Sina Nia Kosari. As our final project, my partners Oliver and Marcin and I developed a haptic enabled glove that interfaces with a Microsoft Kinect and the musical synthesis program SuperCollider for controlling sound effects. A picture of the initial prototype of the glove is shown in Figure 25.

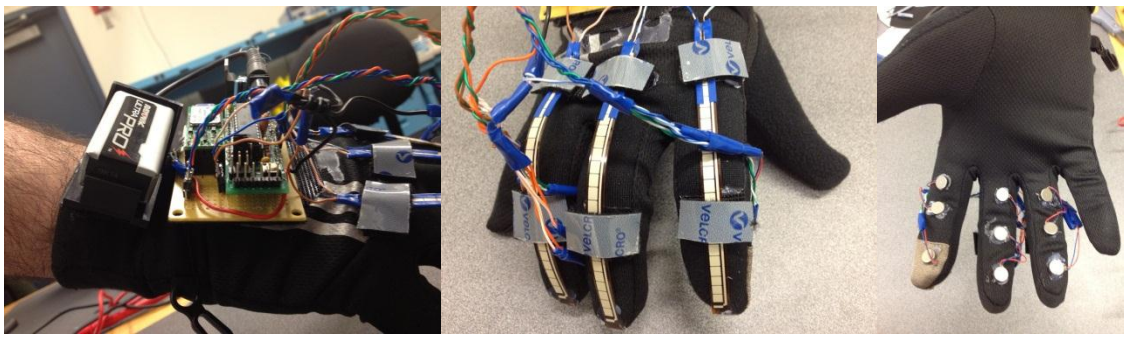

Figure 25: Haptic glove with flex resistors, vibration motors, an Arduino, and Bluetooth for interfacing with a Microsoft Kinect and the music synthesis program SuperCollider.

This project is now being expanded as a larger haptic interface research effort. Eventually we hope that the glove will find general utility in a number of Microsoft Kinect interfaced haptics projects. The video of our initial glove implementation will be provided as supplementary material. A second version of this glove has been developed as part of Professor Chizeck's EE 449 senior design course in the Department of Electrical Engineering for conveying vibrational feedback when in contact with virtual objects.

Undergraduate Research Symposium Presentation

This year I had the opportunity to present my research at the Undergraduate Research Symposium. Thank you to everyone in the BRL for their feedback on my practice sessions. I will make the PowerPoint presentation available in as part of the supplementary materials.

References

1. Yamamoto, T., *Applying Tissue Models in Teleoperated Robot-Assisted Surgery*, in *Mechanical Engineering*2011, The John Hopkins University: Baltimore, Maryland. p. 230.
2. Camacho, E.F. and C. Bordons, *Model predictive control*, 1999, London : Springer Verlag. p. 4.
3. Talamini, M.A., et al., *A prospective analysis of 211 robotic-assisted surgical procedures.* Surgical Endoscopy, 2003. **17**(10): p. 1521.
4. De, S., et al. *Assessment of Tissue Damage due to Mechanical Stresses*. in *Biomedical Robotics and Biomechatronics, 2006. BioRob 2006. The First IEEE/RAS-EMBS International Conference on Biomedical Robotics and Biomechatronics*. 2006.
5. Patel, H.R.H., A. Linares, and J.V. Joseph, *Robotic and laparoscopic surgery: Cost and training.* Surgical Oncology, 2009. **18**(3): p. 242.
6. Fung, Y.C., *Biomechanics: Mechanical Properties of Living Tissues*. 2 ed1993, New York, NY: Springer-Verlag.
7. Yamamoto, T., et al. *Tissue property estimation and graphical display for teleoperated robot-assisted surgery*. in *Robotics and Automation, 2009. ICRA '09. IEEE International Conference on*. 2009.
8. Grant, I.H.W.M., *Recursive Least Squares.* Teaching Statistics, 1987. **9**(1): p. 15.
9. E. A. Wan, R.v.d.M., *Chapter 7: The Unscented Kalman Filter*, in *Kalman Filtering and Neural Networks*, E.S. Haykin, Editor 2001, Wiley Publishing. p. 50.
10. Haddadi, A. and K. Hashtrudi-Zaad. *A new method for online parameter estimation of Hunt-Crossley environment dynamic models*. in *Intelligent Robots and Systems, 2008. IROS 2008. IEEE/RSJ International Conference on*. 2008.
11. Chatelin, S., et al., *In vivo liver tissue mechanical properties by transient elastography: Comparison with dynamic mechanical analysis.* Biorheology, 2011. **48**(2): p. 75-88.
12. J. Ophir, S.A., B. Garra, F. Kallel, E. Konofagou, T. Krouskop, C. Merritt, R. Righetti, R. Souchon, S. Srinivasan, T. Varghese, *Elastography: Imaging the Elastic Properties of Soft Tissues with Ultrasound.* Journal of Medical Ultrasonics, 2002. **29**: p. 155-171.
13. Valtorta, D. and E. Mazza, *Dynamic measurement of soft tissue viscoelastic properties with a torsional resonator device.* Medical Image Analysis, 2005. **9**(5): p. 481-490.
14. Koo, T.K., J.H. Cohen, and Y. Zheng, *A Mechano-Acoustic Indentor System For In Vivo Measurement of Nonlinear Elastic Properties of Soft Tissue.* Journal of manipulative and physiological therapeutics, 2011.
15. Barbé, L., et al., *Needle insertions modeling: Identifiability and limitations.* Biomedical Signal Processing and Control, 2007. **2**(3): p. 191-198.
16. S. Mira, K.B.R., B.W. Schafer, K.T. Remesh, A.M. Okamura, *Mechanics of Flexible Needles Robotically Steered through Soft Tissue.* The International Journal of Robotics Research, 2010. **29**(13): p. 1640-1660.
17. Schwartz, J.-M., et al., *Modelling liver tissue properties using a non-linear visco-elastic model for surgery simulation.* Medical Image Analysis, 2005. **9**(2): p. 103.

18. Carter, F.J., et al., *Measurements and modelling of the compliance of human and porcine organs.* Medical Image Analysis, 2001. **5**(4): p. 231.

19. An, B. and J. Kim, *Dynamic measurement and modeling of soft tissue behavior with an indentation device using indenters of various shapes*, 2006, Trans Tech Publications. p. 781.

20. Tay, B.K., K. Jung, and M.A. Srinivasan, *In Vivo Mechanical Behavior of Intra-abdominal Organs.* Biomedical Engineering, IEEE Transactions on, 2006. **53**(11): p. 2129.

21. Chizeck, H., *Meeting: Issues surrounding the force-displacement measurment device specifications*, A. Hill, Editor 2011.

22. Phillip R Roan, A.S.W.M., Mika N Sinanan MD, Blake Hannaford, *An Instrumented Minimally Invasive Surgical Tool: Design and Calibration.* Applied Bionics and Biomechanics, 2010. **Special Issue on Surgical Robotics**: p. 1.

23. Rosen, J., et al., *Biomechanical Properties of Abdominal Organs In Vivo and Postmortem Under Compression Loads.* Journal of Biomechanical Engineering, 2008. **130**(2): p. 1.

24. Ahn, B. and J. Kim, *Measurement and characterization of soft tissue behavior with surface deformation and force response under large deformations.* Medical Image Analysis, 2010. **14**(2): p. 138.

25. Hu, T. and J. Desai, *A Biomechanical Model of the Liver for Reality-Based Haptic Feedback*, in *Medical Image Computing and Computer-Assisted Intervention - MICCAI 2003*, R. Ellis and T. Peters, Editors. 2003, Springer Berlin / Heidelberg. p. 75.

26. Yamamoto, T., et al. *Techniques for environment parameter estimation during telemanipulation*. in *Biomedical Robotics and Biomechatronics, 2008. BioRob 2008. 2nd IEEE RAS & EMBS International Conference on*. 2008.

27. Eric A. Wan, R.v.d.M., *The Unscented Kalman Filter for Nonlinear Estimation*, in *Adaptive Systems for Signal Processing, Communications, and Control Symposium 2000.*2000, IEEE: Lake Louise, Alta. , Canada

28. Greg Welch, G.B., *An Introduction to the Kalman Filter*, 2006, University of North Caroolina, Chapel Hill: Chapel Hill, NC.

29. Julier, S.J.U., J.K., *Unscented filtering and nonlinear estimation.* Proceedings of the IEEE, 2004. **92**(3): p. 401-422.

30. Kandepu, R., B. Foss, and L. Imsland, *Applying the unscented Kalman filter for nonlinear state estimation.* Journal of Process Control. **18**(7-8): p. 753-768.

31. Stewart, K.O., *Voice coil actuator*, 1994, Aura Systems, Inc: United States of America. p. 1.

32. Howard Chizeck, B.H., *Email: Options for measuring linear displacement*, A. Hill, Editor 2011: Seattle. p. 1.

33. Buttolo, P., *Hard-disk actuators for mini-teleoperation.* Proc. SPIE, 1995. **2351**(1): p. 55.